Research article

Influence of Phase Structure of TiO_2 Nanoparticles on Resistive Switching Devices

Benchapol Tunhoo[1], Direklit Chantarawong[2], Thutiyaporn Thiwawong[1]* and Korakot Onlaor[1]

[1]*Electronics and Control System for Nanodevice Research Laboratory, College of Materials Innovation and Technology, King Mongkut's Institute of Technology Ladkrabang, Bangkok, Thailand*
[2]*School of Engineering, King Mongkut's Institute of Technology Ladkrabang, Bangkok, Thailand*

Curr. Appl. Sci. Technol. 2024, Vol. 24 (No. 2), e0258184; https://doi.org/10.55003/cast.2023.258184

Received: 25 April 2023, Revised: 29 May 2023, Accepted: 3 August 2023, Published: 6 October 2023

Keywords

TiO_2;

nanoparticles;

resistive;

switching;

memory;

PVK

Abstract

In this work, the electrical memory properties of a bi-stable device based on the structure of aluminum/poly (9-vinyl carbazole) (PVK): TiO_2 NPs/indium-tin-oxide (ITO) were reported. The effects of the modified phase structural of titanium dioxide nanoparticles (TiO_2 NPs) on the electrical memory characteristics were determined. The TiO_2 NPs were annealed at different annealing temperatures. The physical properties of the annealed TiO_2 NPs were characterized by transmission electron microscope and X-ray diffraction, which revealed the composition and structure of the anatase and rutile phases. Current-voltage measurements showed that the bi-stable characteristics were affected by the phase structure of the TiO_2 NPs. The ON/OFF current ratio of the fabricated device was noted to be approximately 2.06×10^5 in the case of TiO_2 NPs annealed at 500°C. A theoretical model was used to explain the charge injection mechanisms of the device. Moreover, the temperature dependence and retention-time measurements of the device were demonstrated.

1. Introduction

One metal oxide nanoparticle that has gained attraction in many research fields and applications is titania, or titanium dioxide (TiO_2). Normally, TiO_2 is a well-known material that has increasingly

*Corresponding author: Tel.: (+66) 3298000
E-mail: thutiyaporn.th@gmail.com

attracted research interest for its potential application in many fields due to its excellent features, including electrical, optical, and photocatalytic properties [1]. Typically, TiO_2-based materials exhibit many polymorphic structures with several crystalline phases such as rutile, anatase, brookite, etc. [2]. Typically, the active structural phases of TiO_2 are the rutile and anatase phases, which can be used in various applications [3-5]. P-25 TiO_2 NPs (Degussa) are a commercially available TiO_2 NPs with a large surface area [6]. They are widely used in many applications, such as photocatalysts and sensors [7, 8]. Typically, P-25 TiO_2 is composed of mixed rutile and anatase crystalline structures in a ratio of about 1:3 with individual phase isolation [9]. Differences in structural characteristics affect performance in its applications. In some applications, including photocatalyst applications and oxygen indication, specific phase structures of TiO_2 are required. Moreover, it is well known that the anatase phase demonstrates higher photocatalytic properties than the rutile phase [10]. The anatase phase exhibits a metastable phase, while the rutile possesses a stable structure phase. The phase transformation from the anatase to the rutile structures of TiO_2 NPs was studied by several researchers [11], and the transformation was shown to be dependent on the process parameters such as sintering temperature, pressure, and heating rate.

One of the applications that TiO_2 proved to be a significant candidate was the "memristor" device [12, 13]. The memristor or memory resistor is a device that remembers data in terms of electrical device resistance [14-16]. Recently, many materials have been used to prepare the memristors, including metal oxides, carbon-based materials, and organic materials [17]. Composite materials of metal oxide nanoparticles and polymer materials have attracted significant interest in studying the application of novel memory and resistive switching devices due to their excellent properties such as a simple preparation process, low cost, and low power consumption [18-22]. The behavior of TiO_2 in the field of memristors has been studied for modern applications such as resistive random-access memory (RRAM), biohybrid systems, and sensing devices. The switching characteristics of embedded TiO_2 in polymer matrices have been widely studied [23-25]. The charge transfer from TiO_2 NPs to polymer material plays a key role in the operation of the device. In several reports, embedded TiO_2 in polymer memristors demonstrated various conduction mechanisms, which depended on the kind of polymer used and the properties of the TiO_2 material. Cho *et al.* [23] reported on the bi-stable characteristics of Al/poly (N-vinylcarbazole) (PVK): TiO_2/indium tin oxide (ITO) devices, which demonstrated a filamentary conduction mechanism. Ghosh and Pal [26] had been reported the redox-driven mechanism of the bi-stable device of ITO/poly (3-hexylthiophene) (P3HT): TiO_2/Al. It has been well established that the structural properties, such as the crystalline phase, have affected the charge transfer of TiO_2 NPs. However, studies of the structural properties of TiO_2 NPs in composite polymer materials for memristor devices are few.

In this work, the effects of TiO_2 NPs phase composition on the properties of a bi-stable device were studied. P-25 TiO_2 NPs were annealed at different temperatures. Then, poly (9-vinyl carbazole) (PVK) was composited with the annealed TiO_2 NPs to fabricate a bi-stable device. The influence of the structural properties of the annealed TiO_2 NPs on the electrical bistability of the polymer composite devices was investigated.

2. Materials and Methods

Commercial P-25 TiO_2 NPs (Sigma Aldrich Co.) were used as starter material. TiO2 NPs were annealed in ambient conditions at temperatures of 500°C, 700°C, and 900°C for 2 h to observe the influence of thermal annealing temperature. X-ray diffraction (XRD) technique with a Cu $\kappa\alpha$ (λ= 0.1542 nm) radiation source (Rigaku SmartLab) was used to assess the crystalline structural properties of TiO_2 NPs. Transmission electron microscopy (TEM, FEI Tecnai G2 20) was applied to perform the particle size of the annealed TiO_2 NPs. Before preparing the device, PVK that had been dissolved in chlorobenzene solvent was used as polymer blending material in the bi-stable device. The concentration of PVK and chlorobenzene was kept at 10 mg/mL. TiO_2 NPs prepared at different annealing temperatures (500°C, 700°C, and 900°C) were blended into the solution of PVK in chlorobenzene at a concentration of 9 wt% with ultrasonication for 10 min. Then, each mixed solution of PVK: TiO_2 NPs was coated on an indium tin oxide (ITO)/glass substrate by spin coating at a speed of 2000 rpm for 30 s. After that, the films were baked at 80°C to remove any solvent. A 100 nm aluminum (Al) film was deposited on the PVK: TiO_2 NPs film as a top electrode by the vacuum thermal deposition process. A field emission scanning electron microscope (FEM, JEOL JSM-7001F) was used to capture the surface morphology and thickness of the prepared films. The current-voltage characteristics (I-V) were measured by a source meter (Keithley 2410) to assess each device's electrical properties under ambient conditions. The measurement was controlled by a computer program.

3. Results and Discussion

Figure 1 depicts the XRD diffraction spectra of the annealed TiO_2 NPs prepared at various annealing temperatures. The patterns on the XRD spectra exhibit the phase structures of both the rutile (R) and anatase (A) phases. The most organic compounds in starter TiO_2 particles were gradually disappeared at the above annealing temperature, while the structural phases of TiO_2 remained as pristine P-25 TiO_2 [27]. It was found that the composition of the structural phase depended on the annealing temperature [28, 29]. To identify the composition phase of TiO_2 NPs, the relative weight fractions were calculated from the XRD results. The weight fraction of the rutile phase (W_R) and anatase phase (W_A) can be calculated with the intensity of XRD spectra using the following equations [28]:

$$W_R = 1/(1 + 0.8 I_A / I_R) \tag{1}$$

$$W_A = 1/(1 + 1.26 I_R / I_A) \tag{2}$$

Where I_A is the integrated intensity of the anatase phase at the (101) plane, and I_R is the integrated intensity of the rutile phase at the (110) plane. From the XRD spectra, a de-convolution of anatase and rutile peaks was performed to calculate the phase weight fractions. Table 1 shows the calculated values of W_R and W_A weight fractions. At an annealing temperature of 500°C, the anatase and rutile phase weight fractions were 87.01% and 12.89%, respectively. These values were closed to the ratios for the rutile and anatase phases for P-25 TiO_2 NPs reported in other work [29]. In the case of the annealing temperature of 700°C, it was found that the phase structure of TiO_2 NPs had been converted from a mixed phase of anatase-rutile to a majority rutile phase with the weight fractions of anatase and rutile phases at 8.26% and 91.67%, respectively. While for TiO_2 NPs annealed at 900°C, almost all the anatase phase in TiO_2 NPs was transformed to the rutile structure phase, as shown in Table 1. Hanaor and Sorrell [30] previously reported on the structural transformation of the anatase phase to the rutile phase with heating at temperatures higher than 700°C. Zhang and Banfield [11] reported a kinetic model for TiO_2 phase transformation, which featured the interface nucleation of neighboring anatase particles and the growth of rutile nuclei. The transformation kinetics of anatase to rutile phase depend on the anatase particles' numeric fraction. In addition, the supply of thermal energy is an important parameter. It was shown that the formation of a stable nucleus product depends on the parameter of interfacial energy such as temperature, heating rate, reacting time, etc. In addition, Galizia *et al*. [31] reported that the parameters such as heating rate

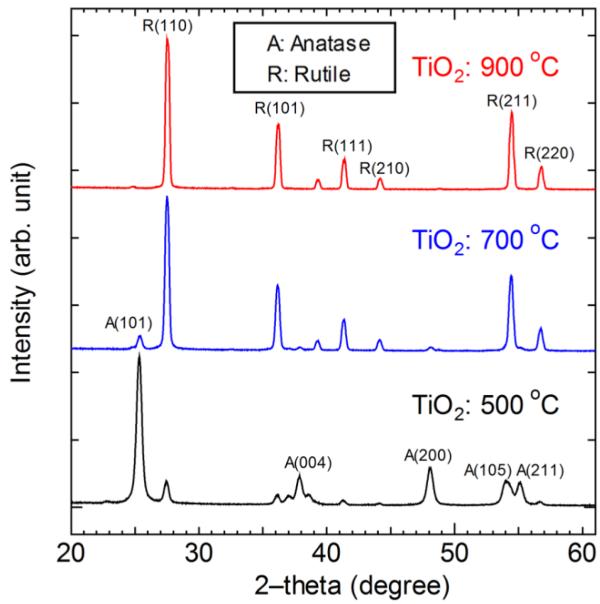

Figure 1. X-ray diffraction pattern at various annealing temperatures

Table 1. The anatase and rutile phase compositions of the P-25 TiO_2 NPs at various annealing temperatures

Annealing temperature (°C)	W_R	W_A
500	12.89%	87.01%
700	91.67%	8.26%
900	99.34%	0.65%

were significant in the transformation to rutile phase. The phase transformation depends on the supply of thermal energy and annealing time. In addition, the physical parameters such as contact points of anatase phase in nanoparticles affected the behavior of phase transform. The high order of phase transform from anatase to rutile phase can be achieved in the nanoparticles of closed space of anatase-anatase contact points because the closer space in particles might change the supply thermal energy to transform the phase of annealing particles. Typically, the material's structural properties, such as electrical and optical properties, affect physical features. Therefore, the influence of temperature on the annealing of TiO_2 NPs for the electrical bi-stable properties of the device was reported.

Figure 2 illustrates bright field images of the TiO_2 NPs from transmission electron microscope at various annealing temperatures. The annealed TiO_2 NPs were found to be present as small particles at 500°C, as shown in Figure 2(a). With the raising of the annealing temperature, the size of the annealed TiO_2 NPs increased, as shown in Figure 2(b and c). The effect of annealing temperature on the morphology of TiO_2 NPs was reported in other work [32]. The surface area of TiO_2 NPs declined due to the influence of the annealing process, which induced the agglomeration of nanoparticles during the treatment process. Figure 3 depicts the surface morphology of prepared TiO_2: PVK films. In the case of 500°C TiO_2, fine particles were found over the surface. This might

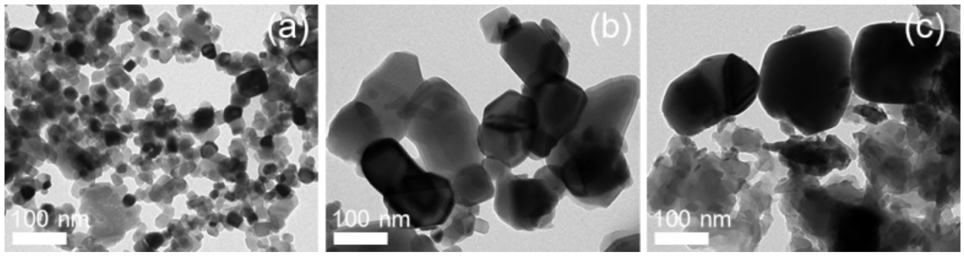

Figure 2. TEM images at different annealing temperatures (a) 500 °C, (b) 700 °C, and (c) 900°C

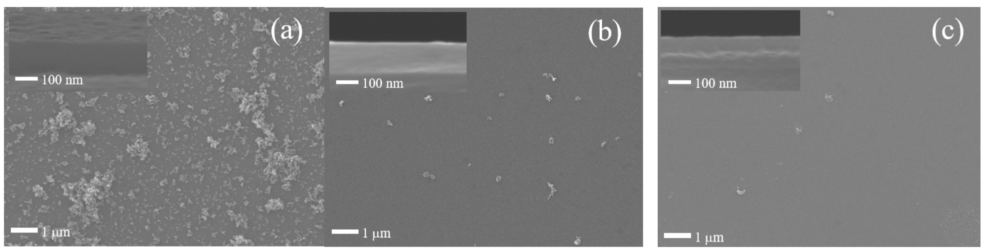

Figure 3. FESEM surface morphology images of TiO_2: PVK films with TiO_2 NPs annealing temperatures of (a) 500°C, (b) 700°C, and (c) 900°C; inset of each image shows the cross-sectional view to obtain the thickness of prepared films.

be because of the fine particle size under these conditions. In the other films, it can be seen that the prepared TiO_2: PVK film exhibited a smooth surface without cracking, which was more suitable for use in the device. In addition, the inset of each image showed the cross-sectional view used to obtain the thickness of prepared films. Ten points of the image were used to estimate the thickness of the film. The thicknesses of TiO_2: PVK films at the different TiO_2 NPs annealing temperatures of 500°C, 700°C, and 900°C were 148±5.51, 136.58±4.38, and 142.63±5.88 nm, respectively.

A schematic of the complete device is shown in the inset of Figure 4(a). The PVK: TiO_2 NPs memory devices with P-25 TiO_2 NPs were tested with various TiO_2 NPs concentrations to find the optimal loading conditions. Figure 4 depicts the I-V characteristics of the devices at different concentrations. The ON/OFF current ratios of 0, 5, 9, 15 wt% at +1 V were 10.4, 1.03×10^4, 2.06×10^5 and 6.00×10^2, respectively. The data indicated that TiO_2 NPs at a loading concentration of 9 wt% gave the highest ON/OFF current ratio. However, the ON/OFF current ratio decreased when the TiO_2 NPs were increased to 15wt% probably due to the aggregation of TiO_2 NPs. The electrical characteristics were obtained from the current-voltage measurement with sweep voltage from 0 to +3 V (curve 1), +3 to 0 V (curve 2), 0 to -3 V (curve 3), and -3 to 0 V (curve 4). The results showed that low bias voltage from 0 V to +2 V caused the device to exhibit a low current region, defined as the OFF state. When the applied voltage was increased, the current was immediately changed to high current or high conduction condition, called the ON state. After changing state, the injection current was stored in the ON state. Even if the reverse voltage to -3 V was biased to the devices, the device state remained in the ON state. This characteristic corresponded to a write-once-read-many (WORM) memory device [33]. Figure 5. depicts the current-voltage (*I-V)* behaviors of PVK: TiO_2 NPs bi-stable devices at various annealing temperatures of TiO_2 NPs. It was found that the ON/OFF current ratios at a reading voltage of +1 V were 2.06×10^5, 2.57×10^3, and 2.02×10^3 for the annealing temperatures of NPs at 500°C, 700°C, and 900°C, respectively. The highest ON/OFF current ratio of the prepared device was found for TiO_2 NPs annealed at 500°C. These results revealed that the structural properties of TiO_2 NPs clearly influenced the resistive switching behaviors.

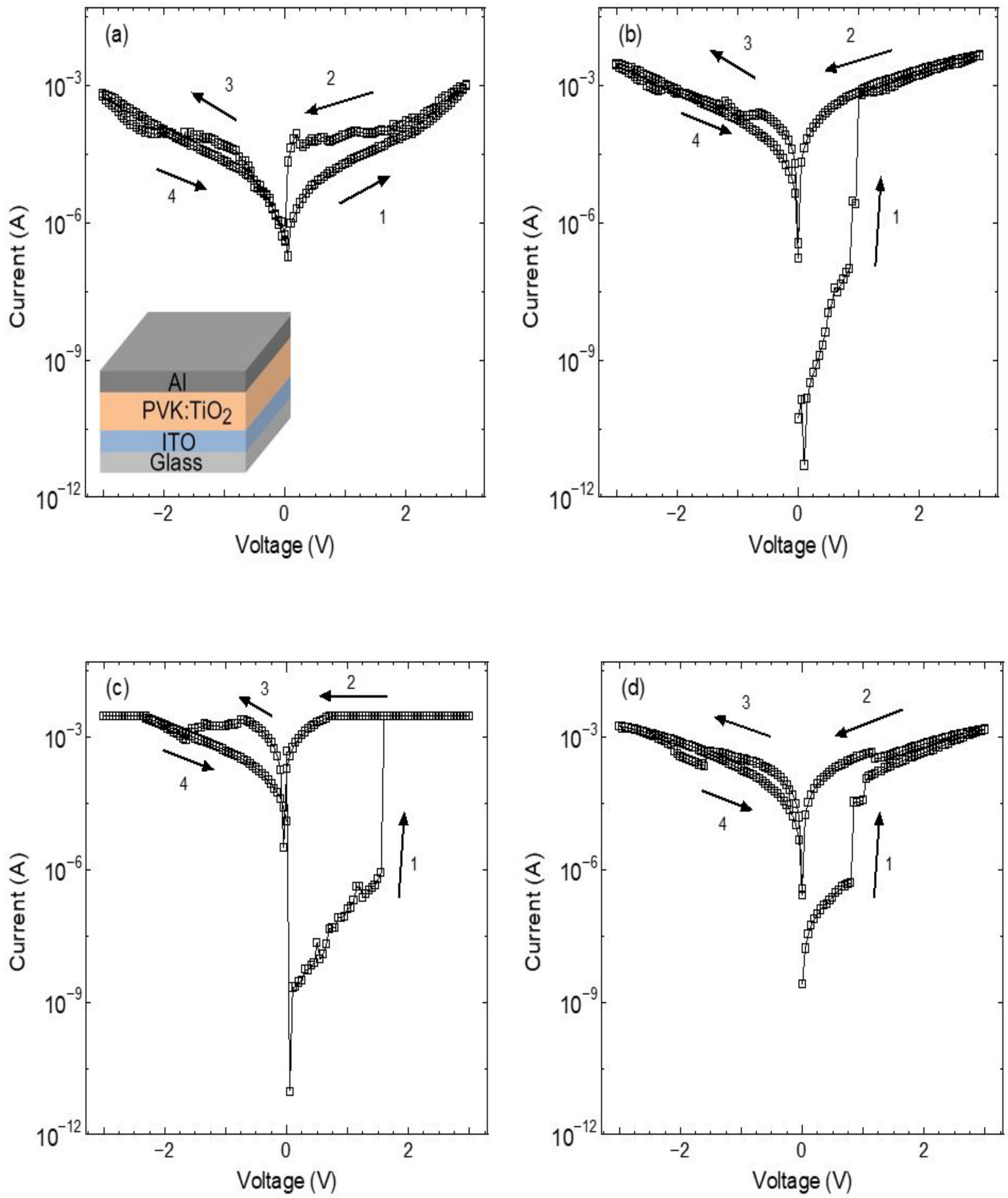

Figure 4. *I-V* characteristics of the device with annealing at 500°C for TiO_2 NP concentrations of (a) 0% wt., (b) 5% wt., (c) 9% wt., and (d) 15 %wt., respectively.

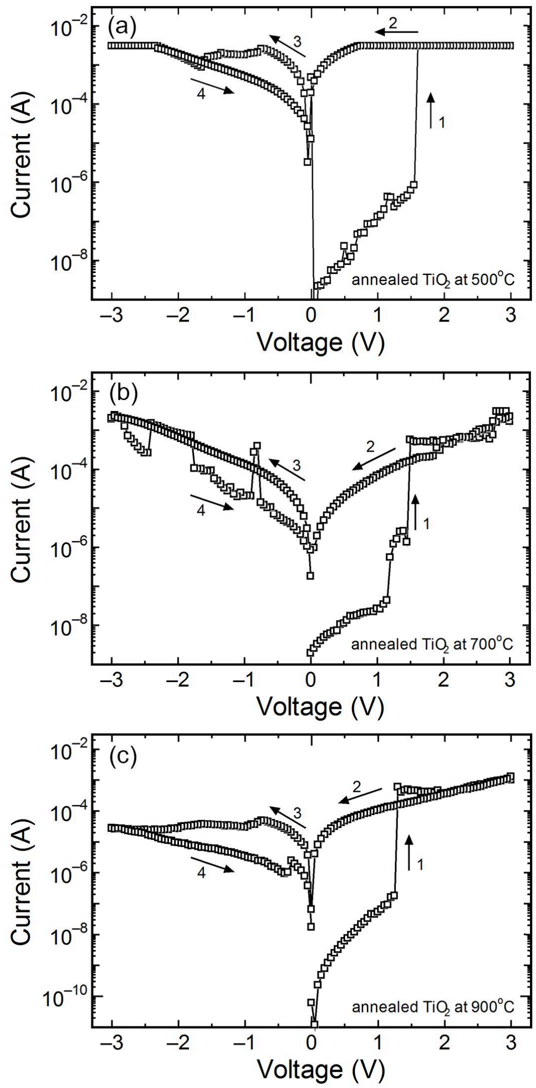

Figure 5. *I-V* characteristics of the device at annealing temperatures of (a) 500°C, (b) 700°C, and (c) 900°C

The results were used to explain the electrical mechanisms of the device. The current-voltage curves of Figure 5 were fitted to theoretical electrical models. Figure 6(a) depicts the results for the current-voltage curve in the region of the OFF state that fitted properly with the conduction theoretical model of thermionic emission [20], expressed as:

$$I = T^2 \exp\left[\frac{-(\phi_b - q\sqrt{qV/4\pi d\varepsilon_i})}{k_b T}\right] \tag{3}$$

where T is the measurement temperature, ϕ_b is the energy barrier height at the interface, ε_i is the permittivity of the sample, q is the charge of electron, k_b is Boltzmann's constant, and d is the thickness of the sample. In this model, the carriers in the OFF state conducted thermal energy activated charge across the potential barrier generally found in polymer conductions [20]. In addition, Figure 6(b) depicts the current-voltage curve in the region of the ON state that fitted properly with Ohmic conduction models usually found in polymers composited with particles [20]. It was found that the fitting results of all devices correlated well with the above models.

For clear information about the mechanisms, the proposed diagrams of the energy bands of the device in various states were presented. The work functions of the bottom ITO and top Al electrodes were -4.6 eV and -4.2 eV, respectively [34, 35]. The energy levels of PVK at LUMO and HOMO are -2.0 eV and -5.5 eV, respectively [36]. For the TiO_2 NPs, the energy band gap values depended on the phase structure of TiO_2 NPs [37]. In previous reports, the conduction band (CB) and valence band (VB) of the TiO_2 anatase phase were -5.10 eV and -8.3 eV, respectively [37]. Meanwhile, the rutile phase of TiO_2 has CB and VB levels at -4.80 eV and -7.83 eV, respectively [37]. One of the acceptable switching mechanisms is the trapping process [36, 38]. However, the ratios between the rutile and anatase phases changed with different annealing temperatures (see Table 1). Therefore, an energy band diagram was determined for two cases: (1) trapping states dominated by the anatase phase, as shown in Figures 7(a), and (2) trapping states dominated by the rutile phase, as shown in Figure 7(b). Nevertheless, both cases exhibited the same mechanisms when voltages were applied. Figure 7(c) depicts the band energy diagram in the region of the OFF state, in which the Al and ITO electrodes were negatively and positively biased, respectively. The positive charges from the ITO electrode were injected into the HOMO of PVK by thermal energy activation.

On the other hand, the negative charges from the Al electrode were injected into LUMO by thermal energy corresponding to thermionic emission. The negative charges were trapped, and the positive charges were blocked by the trapping and blocking states inside the PVK: TiO_2 NPs layer. Figure 7(d) depicts the model of the energy band diagram in the region of the ON state of the prepared device. Electrons filled the trapping states at high voltage bias. Afterwards, the injected electrons could be easily transported to the ITO electrode. Therefore, the state of the prepared device was changed from the OFF to the ON state. Figure 7(e) shows the reverse bias voltages of the device. The PVK prevented electrons from moving out of the trapping states. Therefore, electrons could be transported directly through the device and exhibited the ON state. Considering energy levels, the trapping states of the anatase TiO_2 were deeper than those of the rutile TiO_2. Therefore, deep traps needed more electrons before the trapping states were filled, and the ratio between the OFF and ON states exhibited large ON/OFF current ratios. In addition, the devices dominated by the rutile phase showed shallow traps. Therefore, the traps were more easily filled by electrons, and the device showed low writing voltage, as seen in Figures 5(b) and 5(c). It was found that the dominant rutile phase occurred at both annealing temperatures of 700°C and 900°C. Thus, the values of the ON and OFF states led to a lower value of the ON/OFF current ratio than the device dominated by the anatase phase.

Figure 8(a) depicts the current-voltage curve measurement of the prepared device at different temperatures from room temperature to 90°C. It was found that the ratio of ON/OFF current states decreased with rising measurement temperatures. The decrease of the ON/OFF current ratio was significantly altered in the OFF state. In addition, the currents in the OFF state at +1 V were used to examine the device mechanisms. Figure 8(b) shows a typical Arrhenius plot that can be used to explain the estimation of the OFF-state current. The data were fitted and showed the linearity, confirming the thermionic emission model for the OFF state. Moreover, the activation energy of the trapping centers of the annealed P-25 TiO_2 NPs at 500°C for the device was approximately 1.15 eV, as determined from the slope.

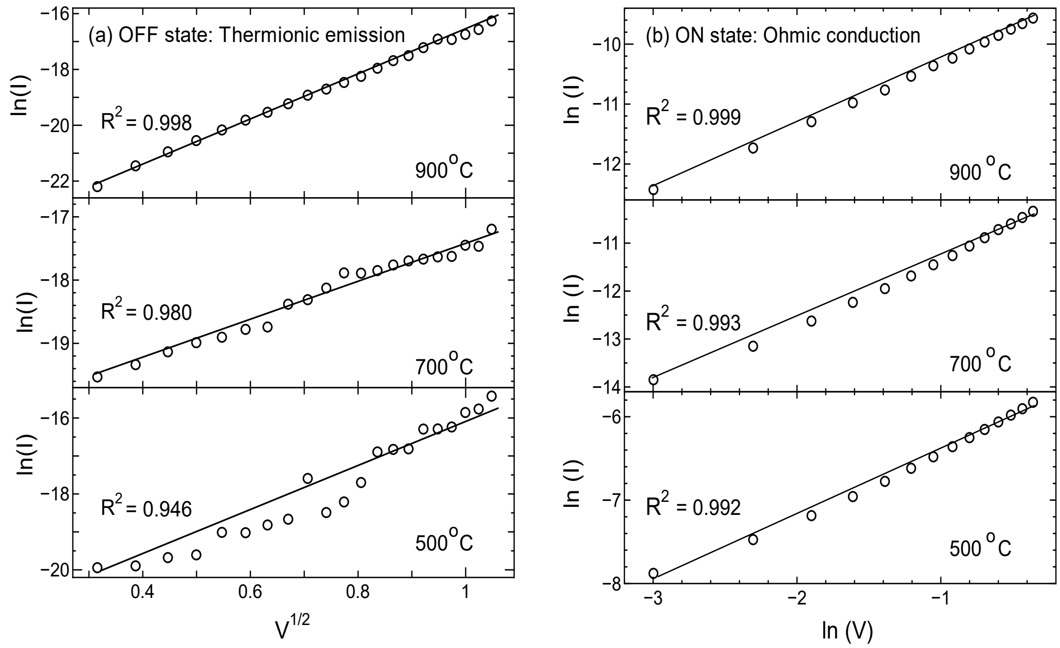

Figure 6. Theoretical fitting model of the TiO_2: PVK bi-stable device at (a) OFF state and (b) ON state regions

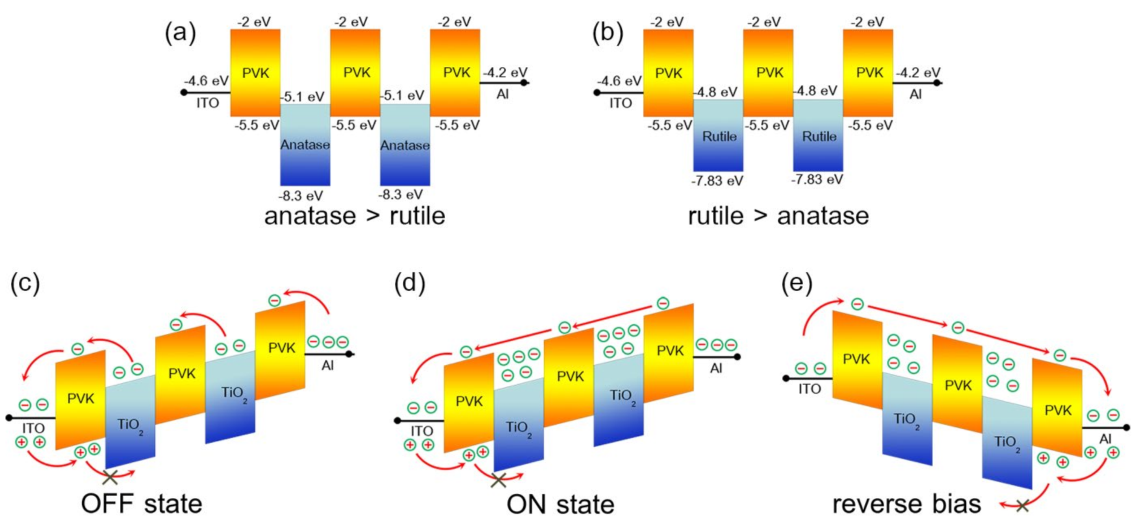

Figure 7. Energy band diagram for bi-stability behaviors of TiO_2 NPs composited with PVK polymer memory device

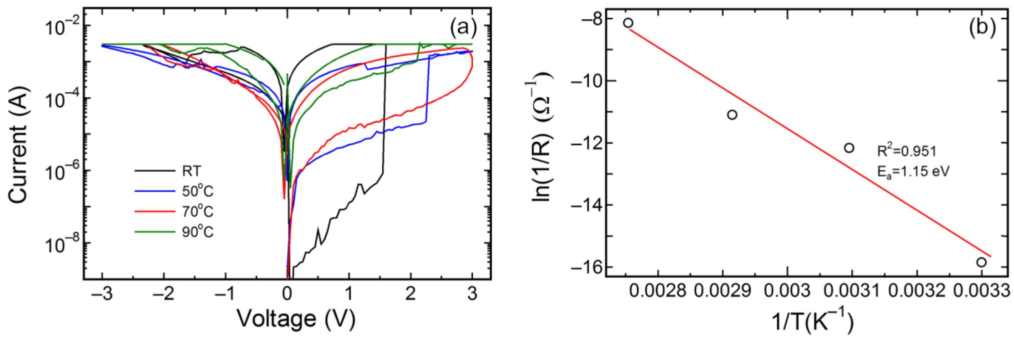

Figure 8. Temperature measurement of the device for P-25 TiO_2 NPs annealed at 500°C, (a) *I-V* temperature dependent characteristics, and (b) Arrhenius plot of the device operating in the OFF state at device bias of +1 V

Retention is another parameter used to indicate the performance of a bi-stable memory device. At first, a +1 V reading voltage was applied and the current of the device was measured at the same time for 6 h to obtain the retention property, which defined the OFF-state region. Then, a single pulse of +3 V was applied to the device as a trigger signal for the writing step. It was found that the writing voltage changed the state of the device from OFF to ON states. After that, the current of the device was collected at a voltage of +1 V for 6 h, which was defined as the ON state region. Figure 9 illustrates the retention characteristics of the optimal condition for TiO_2 NPs annealed at 500°C. It was found that the prepared device exhibited high stability in the ON state and fluctuation in the OFF state. This fluctuation behavior might be an effect of the positive charges that were activated through the block barrier with the environmentally thermal energy in the OFF state. In comparison with other research, the features of our bi-stable device are shown in Table 2. Therefore, the bi-stable device with ITO/PVK: TiO_2 NPs/Al structure demonstrated a high ratio of ON/OFF current ratio with stable time-retention behavior.

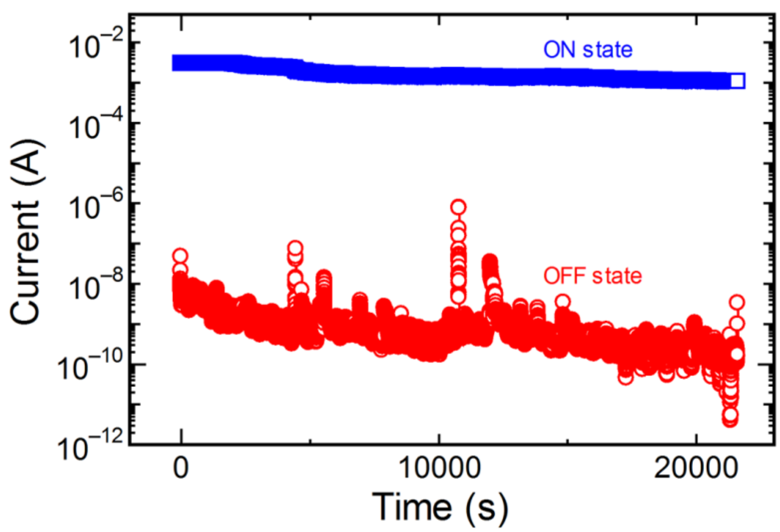

Figure 9. Time retention measurement of TiO_2: PVK NPs bi-stable device

Table 2. Example of the device parameters of various metal oxide nanoparticle polymer composited bi-stable devices

Device Structure	ON/OFF Current Ratio	Retention Time	Reading Voltage	Ref.
FTO/TiO_2-PVA/Ag	5×10^3	n/a	+2 V	[39]
GaIn/PFBT−TiO_2 NPs/ITO/PET	10^3	n/a	+0.5 V	[40]
GaIn/PVK-TiO_2 NPs/Cu	10^3	10 years[1]	n/a	[41]
Al/PVA: TNTs/FTO	10^4	1×10^4 s	+0.1 V	[20]
ITO/PVK-TiO_2 NPs/Al	2×10^5	2×10^4 s	+1 V	This work

[1]Extrapolated to 10 years

4. Conclusions

We successfully studied the effects of annealing temperatures of P-25 TiO_2 NPs on the electrical bi-stability of a resistive switching device. The P-25 TiO_2 NPs were annealed at the temperatures of 500°C, 700°C, and 900°C for 2 h in a furnace. The crystallite structure of resulting TiO_2 NPs was a mixture of anatase and rutile phases but was transformed into predominantly rutile phase at higher annealing temperatures. The weight fractions of the anatase and rutile phases at different annealing temperatures were calculated. A bi-stable device was fabricated on the Al/TiO_2: PVK/ITO device structure. With current-voltage measurement, the fabricated devices exhibited two electrical states with different current values. For the device, an optimal condition of TiO_2 NPs was obtained at 500°C annealing temperature and a TiO_2 NPs concentration of 9% by weight of PVK. The highest ON/OFF current ratio was observed at 2.06×10^5 at a reading voltage of +1 V. To better explain the device mechanism, the thermionic emission and Ohmic conduction charge transfer models were proposed to describe the device behavior in the OFF and ON states by fitting to current-voltage results. Furthermore, the device mechanisms were confirmed with temperature-dependent measurements at different temperatures, ranging from room temperature to 90°C. Moreover, the device was tested with time-retention measurement to perform practical applications. The prepared device exhibited high stability in the ON state and the OFF state for more than 6 h.

5. Acknowledgements

The research received funding support from NRNF (KMITL grant number: RE-KRIS/FF65/39). The authors acknowledge facilities and technical assistance from the Nanotechnology and Materials Analytical Instrument Service Unit (NMIS) of the College of Materials Innovation and Technology, King Mongkut's Institute of Technology Ladkrabang.

References

[1] Kalaivani, T. and Anilkumar, P., 2018. Role of temperature on the phase modification of TiO_2 nanoparticles synthesized by the precipitation method. *Silicon,* 10(4), 1679-1686.

[2] Rath, C., Mohanty, P., Pandey, A.C. and Mishra, N.C., 2009. Oxygen vacancy induced structural phase transformation in TiO_2 nanoparticles. *Journal of Physics D: Applied Physics,* 42(20), https://doi.org/10.1088/0022-3727/42/20/205101.

[3] Li, P., Wang, J., Peng, T., Wang, Y., Liang, J., Pan, D. and Fan, Q., 2019. Heterostructure of anatase-rutile aggregates boosting the photoreduction of U (VI). *Applied Surface Science,* 483, 670-676.

[4] Song, W., Jiang, Q., Xie, X., Brookfield, A., McInnes, E.J.L., Shearing, P.R., Brett, D.J.L., Xie, F. and Riley, D.J., 2019. Synergistic storage of lithium ions in defective anatase/rutile TiO_2 for high-rate batteries. *Energy Storage Materials,* 22, 441-449.

[5] Tamgadge, R.M. and Shukla, A., 2018. Fluorine-doped anatase for improved supercapacitor electrode. *Electrochimica Acta,* 289, 342-353.

[6] Ohno, T., Sarukawa, K., Tokieda, K. and Matsumura, M., 2001. Morphology of a TiO_2 photocatalyst (Degussa, P-25) consisting of anatase and rutile crystalline phases. *Journal of Catalysis,* 203(1), 82-86.

[7] Han, E., Vijayarangamuthu, K., Youn, J.-S., Park, Y.-K., Jung, S.-C. and Jeon, K.-J., 2018. Degussa P25 TiO_2 modified with H_2O_2 under microwave treatment to enhance photocatalytic properties. *Catalysis Today,* 303, 305-312.

[8] Trejo-Tzab, R., Alvarado-Gil, J., Quintana, P. and López, T., 2008. Study of the photoactivation of titania Degussa P25 in ethanol–methanol suspensions using a piezoelectric sensor. *Journal of Molecular Catalysis A: Chemical,* 281(1-2), 113-118.

[9] Ohtani, B., Prieto-Mahaney, O.O., Li, D. and Abe, R., 2010. What is Degussa (Evonik) P25? Crystalline composition analysis, reconstruction from isolated pure particles and photocatalytic activity test. *Journal of Photochemistry and Photobiology A: Chemistry,* 216(2-3), 179-182.

[10] Wang, W.-K., Chen, J.-J., Zhang, X., Huang, Y.-X., Li, W.-W. and Yu, H.-Q., 2016. Self-induced synthesis of phase-junction TiO_2 with a tailored rutile to anatase ratio below phase transition temperature. *Scientific Reports,* 6(1), https://doi.org/10.1038/srep.20491.

[11] Zhang, H. and Banfield, J.F., 1999. New kinetic model for the nanocrystalline anatase-to-rutile transformation revealing rate dependence on number of particles. *American Mineralogist,* 84(4), 528-535.

[12] Illarionov, G.A., Morozova, S.M., Chrishtop, V.V., Einarsrud, M.-A. and Morozov, M.I., 2020. Memristive TiO_2: synthesis, technologies, and applications. *Frontiers in Chemistry,* 8, https://doi.org/10.3389/fchem.2020.00724.

[13] Strukov, D.B., Snider, G.S., Stewart, D.R. and Williams, R.S., 2008. The missing memristor found. *Nature,* 453(7191), 80-83.

[14] Salaoru, I., Li, Q., Khiat, A. and Prodromakis, T., 2014. Coexistence of memory resistance and memory capacitance in TiO_2 solid-state devices. *Nanoscale Research Letters,* 9(1), https://doi.org/10.1186/1556-276X-9-552.

[15] Hu, S., Yue, J., Jiang, C., Tang, X., Huang, X., Du, Z. and Wang, C., 2019. Resistive switching behavior and mechanism in flexible TiO_2@ Cf memristor crossbars. *Ceramics International,* 45(8), 10182-10186.

[16] Nafea, S.F., Dessouki, A.A.S., El-Rabaie, S., Elnaghi, B.E., Ismail, Y. and Mostafa, H., 2019. An accurate model of domain-wall-based spintronic memristor. *Integration,* 65, 149-162.

[17] Kim, S.G., Han, J.S., Kim, H., Kim, S.Y. and Jang, H.W., 2018. Recent advances in memristive materials for artificial synapses. *Advanced Materials Technologies,* 3(12), https://doi.org/10.1002/admt.201800457.

[18] Jang J., Park W., Cho K., Song H., and Lee T., 2013. Non-volatile memory characteristics of polyimide layers embedded with ZnO nanowires. *Current Applied Physics,* 13(7), 1237-1240.

[19] Ukakimaparn, P., Chantarawong, D., Songkeaw, P., Onlaor, K., Thiwawong, T. and Tunhoo, B., 2019. Electrical bistable properties of P-25 TiO_2 nanoparticles composited with PVP for memory devices. *Journal of Electronic Materials,* 48(10), 6792-6796.

[20] Pham, N.K., Vu, N.H., Van Pham, V., Ta, H.K.T., Cao, T.M., Thoai, N. and Tran, V.C., 2018. Comprehensive resistive switching behavior of hybrid polyvinyl alcohol and nanotube nanocomposites identified by combining experimental and density functional theory studies. *Journal of Materials Chemistry C,* 6(8), 1971-1979.

[21] Wu, W., Jia, M., Zhang, Z., Chen, X., Zhang, Q., Zhang, W., Li, P. and Chen, L., 2019. Sensitive, selective and simultaneous electrochemical detection of multiple heavy metals in environment and food using a lowcost Fe_3O_4 nanoparticles/fluorinated multi-walled carbon nanotubes sensor. *Ecotoxicology and Environmental Safety,* 175, 243-250.

[22] Pilch, M. and Molak, A., 2014. Resistance switching in rejuvenated $NaNbO_3$: Mn crystals. *Phase Transitions,* 87(10-11), 1114-1128.

[23] Cho, B., Kim, T.-W., Choe, M., Wang, G., Song, S. and Lee, T., 2009. Unipolar nonvolatile memory devices with composites of poly (9-vinylcarbazole) and titanium dioxide nanoparticles. *Organic Electronics,* 10(3), 473-477.

[24] Zhang, Y., Zhao, X., Gao, M., He, Z., Chen, J., Wang, S. and Wang, C., 2022. Ternary resistive switching memory behavior of polycarbazole: TiO_2 nanoparticles-based device. *Thin Solid Films,* 754, https://doi.org/10.1016/j.tsf.2022.13921.

[25] Zhang, C., Yu, P.-L., Li, Y. and Li, J.-C., 2020. Polymer/TiO_2 nanoparticles interfacial effects on resistive switching under mechanical strain. *Organic Electronics,* 77, https://doi.org/10.1016/j.orgel.2019.105528.

[26] Ghosh, B. and Pal, A.J., 2009. Conductance switching in TiO_2 nanorods is a redox-driven process: evidence from photovoltaic parameters. *The Journal of Physical Chemistry C,* 113(42), 18391-18395.

[27] Gupta, S.M. and Tripathi, M., 2011. A review of TiO_2 nanoparticles. *Chinese Science Bulletin,* 56(16), 1639-1657.

[28] Sun, H., Peng, T., Liu, B. and Xian, H., 2015. Effects of montmorillonite on phase transition and size of TiO_2 nanoparticles in TiO_2/montmorillonite nanocomposites. *Applied Clay Science,* 114, 440-446.

[29] Castrejón-Sánchez, V.H., López, R., Ramón-González, M., Enríquez-Pérez, Á., Camacho-López, M. and Villa-Sánchez, G., 2018. Annealing control on the anatase/rutile ratio of nanostructured titanium dioxide obtained by sol-gel. *Crystals,* 9(1), https://doi.org/10.3390/cryst9010022.

[30] Hanaor, D.A. and Sorrell C.C., 2011. Review of the anatase to rutile phase transformation. *Journal of Materials science,* 46(4), 855-874.

[31] Galizia, P., Maizza, G. and Galassi, C., 2016. Heating rate dependence of anatase to rutile transformation. *Processing and Application of Ceramics,* 10(4), 235-241.

[32] Porter, J.F., Li, Y.-G. and Chan, C.K., 1999. The effect of calcination on the microstructural characteristics and photoreactivity of Degussa P-25 TiO_2. *Journal of Materials Science,* 34(7), 1523-1531.

[33] Qu, B., Lin, Q., Wan, T., Du, H., Chen, N., Lin, X. and Chu, D., 2017. Transparent and flexible write-once-read-many (WORM) memory device based on egg albumen. *Journal of Physics D: Applied Physics,* 50(31), https//doi.org/10.1088/1361-6463/aa76d6.

[34] Bory, B.F., Gomes, H.L., Janssen, R.A., de Leeuw, D.M. and Meskers, S.C., 2015. Electrical conduction of LiF interlayers in organic diodes. *Journal of Applied Physics,* 117(15), https://doi.org/10.1063/1.4917461.

[35] Whitcher, T.J., Talik, N.A., Woon, K., Chanlek, N., Nakajima, H., Saisopa, T. and Songsiririthigul, P., 2014. Determination of energy levels at the interface between O_2 plasma treated ITO/P3HT: PCBM and PEDOT: PSS/P3HT: PCBM using angular-resolved x-ray and ultraviolet photoelectron spectroscopy. *Journal of Physics D: Applied Physics,* 47(5), https://doi.org/10.1088/0022-3727/47/5/055109.

[36] Son, D.I., Park, D.H., Kim, J.B., Choi, J.-W., Kim, T.W., Angadi, B., Yi, Y. and Choi, W.K., 2011. Bistable organic memory device with gold nanoparticles embedded in a conducting poly (N-vinylcarbazole) colloids hybrid. *The Journal of Physical Chemistry C,* 115(5), 2341-2348.

[37] Scanlon, D.O., Dunnill, C.W., Buckeridge, J., Shevlin, S.A., Logsdail, A.J., Woodley, S.M., Catlow, C.R.A., Powell, M., Palgrave, R.G. and Parkin, I.P., 2013. Band alignment of rutile and anatase TiO_2. *Nature materials,* 12(9), 798-801.

[38] Jyoti, Krylov, P., Berestennikov, A., Aleshin, A., Komolov, A., Shcherbakov, I., Petrov, V. and Trapeznikova, I., 2015. Switching and memory effects in composite films of semiconducting polymers with particles of graphene and graphene oxide. *Physics of the Solid State,* 57(8), 1678-1684.

[39] Jyoti, Kaur, R., Singh, S., Sharma, J. and Tripathi, S.K., 2019. Effect of TiO_2 Concentration on the Non-Volatile Memory Behavior of TiO_2-PVA Polymer Nanocomposites. *Journal of Electronic Materials,* 48(9), 5995-6002.

[40] Li, J.-C., Sui, W. and Li, Y., 2018. Interfacial effects on resistive switching of vacuum spray deposited polymer thin films embedded with TiO_2 nanoparticles under bending strain. *Organic Electronics,* 61, 170-176.

[41] Li, J.-C., Zhang, C. and Shao, S.-J., 2018. Effect of bottom electrode materials on resistive switching of flexible poly (N-vinylcarbazole) film embedded with TiO_2 nanoparticles. *Thin Solid Films,* 664, 136-142.